Available online at www.sciencedirect.com
SCIENCE DIRECT®
Composite Structures 69 (2005) 429–435
COMPOSITE STRUCTURES
www.elsevier.com/locate/compstruct

Two-dimensional and axisymmetric unit cell models in the analysis of composite materials

Nao-Aki Noda [a,*], Hironobu Nisitani [b], Yasushi Takase [a], Yasu-Aki Shukuwa [a]

[a] Department of Mechanical Engineering, Kyushu Institute of Technology, 1-1, Sensui-cho, Tobata, Kitakyushu 804-8550, Japan
[b] Department of Mechanical Engineering, Kyushu Sangyo University, 2-3-1, Matsukadai, Higashi-ku, Fukuoka 8130004, Japan

Abstract

Unit cell models have been widely used for investigating fracture mechanisms and mechanical properties of composite materials assuming periodically arrangement of inclusions in matrix. It is desirable to clarify the geometrical parameters controlling the mechanical properties of composites because they usually contain randomly distributed particulate. To begin with a tractable problem this paper focuses on the effective Young's modulus E of heterogeneous materials. Then, the effect of shape and arrangement of inclusions on E is considered by the application of FEM through examining three types of unit cell models assuming 2D and 3D arrays of inclusions. It is found that the projected area fraction and volume fraction of inclusions are two major parameters controlling effective elastic modulus of inclusions.

Keywords: Mechanical properties; Computational modelling; Finite element analysis; Numerical analysis

1. Introduction

To investigate mechanical properties and ductile fracture mechanisms of structural materials under tension, finite element analyses have been widely used together with unit cell models as shown in Fig. 1(a) and (b) on the assumption of periodically arrangement of voids, particles, inclusions, and fibers in matrix. In the previous studies, for example, Needleman [1] discussed void growth and coalescence using a doubly periodic square array of circular cylindrical voids. Tvergaard [2,3] carried out detailed stress analysis for plane strain and axisymmetric unit cell models (see Fig. 2) considering shear band instabilities in a void containing medium. Christman–Needleman–Suresh [4] also used these two models to investigate the dependence of tensile properties on the matrix microstructures of whisker- and particulate-reinforced metal–matrix composites. In addition, several other researchers investigated these types of composites using similar unit cell models [5–9].

However, unit cell models used in the previous studies always assume periodically arrangement of 'inclusions' having the same shape and dimensions. If the arrangement or shape of inclusions change even a little, the results may be different from the ones shown in the papers. From this viewpoint, it appears to be important to clarify the geometrical parameters controlling the mechanical properties because they usually contain disordered distributed particulate. To begin with a tractable problem, in this paper, we will focus on the effective Young's modulus, which is one of the most important and fundamental properties of composites. Then, we will discuss controlling parameters through examining three types of models in Fig. 1 with varying

* Corresponding author. Tel.: +81 93 884 3124; fax: +81 93 884 3124.
E-mail address: noda@mech.kyutech.ac.jp (N.-A. Noda).

0263-8223/$ - see front matter © 2004 Published by Elsevier Ltd.
doi:10.1016/j.compstruct.2004.08.034

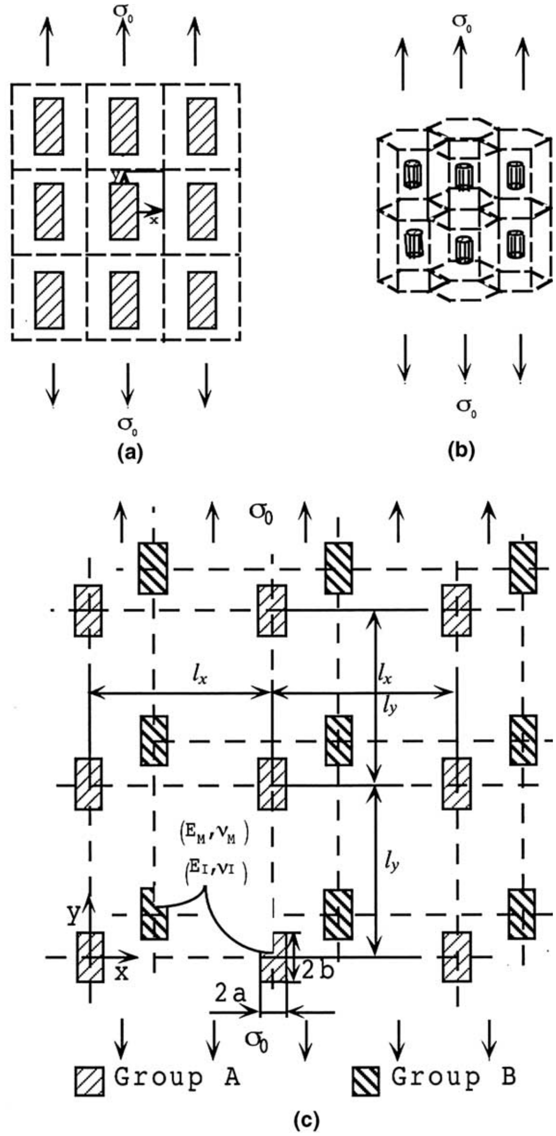

Fig. 1. Three kinds of unit cell models considered (a) 2D model (b) 3D model (c) two-groups-inclusion model both having identical inclusions.

the shape and arrangement of inclusions on the basis of mechanical and physical consideration.

2. Analysis of unit cell models

To predict effective properties of heterogeneous materials from a knowledge of constituents is a classical problem in science and engineering, attracting the attention of a lot of researchers [9–14]. Recently, some investigations have been made for disordered array using such as homogenization method [15–17]. These results are useful for evaluating the actual composites; however, if the shape and arrangement of inclusions are changed a little, we have to reconsider the effective properties. In other words, there is little discussion about the difference between the results of simple models and random

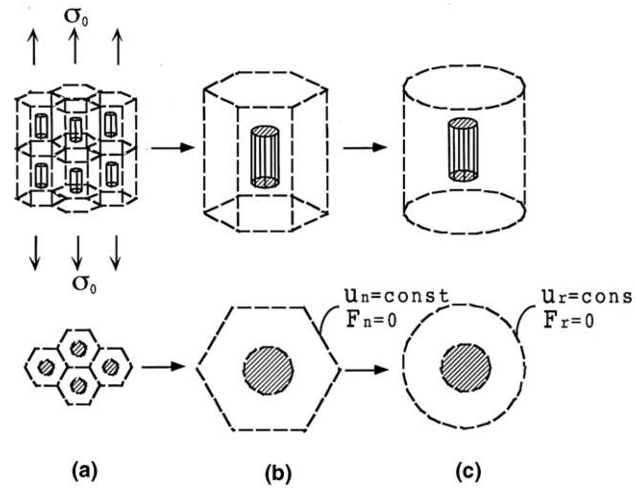

Fig. 2. Axisymmetric unit cell model approximate to 3D array of inclusions.

arrangement in actual composites in terms of mechanics or physics of solids. In this study effective Young's modulus will be considered for three types of models in Fig. 1 by the application of FEM.

As an example, an axisymmetric unit cell model as shown in Fig. 2 can be analyzed in the following way [3]. The boundary conditions of Figs. 2 and 3(a) can be expressed as

$$\begin{aligned}
&\text{(I) On } r=0 \text{ and } 0\leqslant z\leqslant l_z: \quad u_r=0, \quad \tau_{rz}=0,\\
&\text{(II) On } r=l_z \text{ and } 0\leqslant z\leqslant l_z: \quad u_r=u_{r0}, \quad \tau_{rz}=0,\\
&\text{(III) On } z=0 \text{ and } 0\leqslant r\leqslant l_r: \quad u_z=0, \quad \tau_{rz}=0,\\
&\text{(IV) On } z=l_z \text{ and } 0\leqslant r\leqslant l_r: \quad u_z=u_{z0}, \quad \tau_{rz}=0.
\end{aligned} \tag{1}$$

Also we have

$$\int_0^{l_r} \sigma_z|_{z=l_r} 2\pi r \mathrm{d}r = \sigma_0 \times \pi l_r^2, \quad \int_0^{l_z} \sigma_r|_{r=l_r} 2\pi r \mathrm{d}z = 0. \tag{2}$$

We have to set the constants u_{r0}, u_{z0} so as to satisfy Eq. (2). However, since they are still unknown, the auxiliary problems will be solved instead of solving the given problem directly. First, the following auxiliary problem (b) shown in Fig. 3(b) is solved under the boundary condition as shown in Eqs. (3) and (4). Here, this C_1 is an arbitrary constant.

$$\begin{aligned}
&\text{(I) On } r=0 \text{ and } 0\leqslant z\leqslant l_z: \quad u_r=0, \quad \tau_{rz}=0,\\
&\text{(II) On } r=l_z \text{ and } 0\leqslant z\leqslant l_z: \quad u_r=0, \quad \tau_{rz}=0,\\
&\text{(III) On } z=0 \text{ and } 0\leqslant r\leqslant l_r: \quad u_z=0, \quad \tau_{rz}=0,\\
&\text{(IV) On } z=l_z \text{ and } 0\leqslant r\leqslant l_r: \quad u_z=c_1, \quad \tau_{rz}=0.
\end{aligned} \tag{3}$$

Then, the resultant force F_1 in the r-direction on the boundaries $r = l_r$ with $0 \leqq z \leqq l_z$, and the resultant force

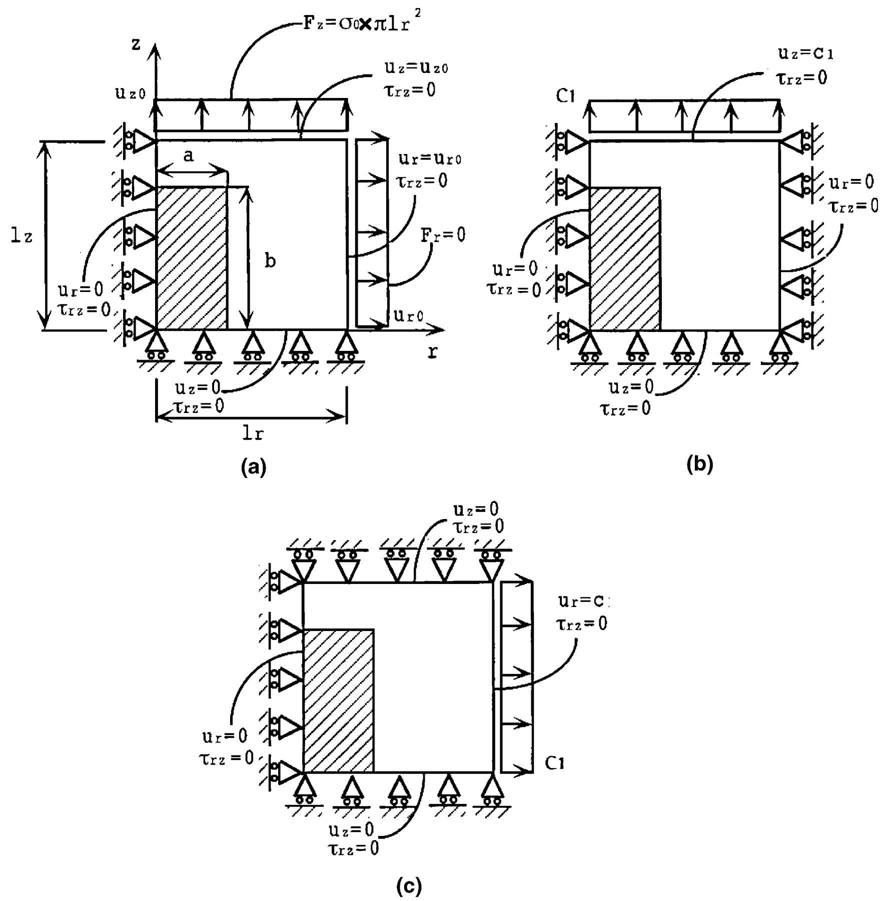

Fig. 3. (a) Given problem for axisymmetric unit cell model, (b), (c) auxiliary problems.

F_2 in z-direction on the boundaries $z = 0$, l_z with $0 \leqq r \leqq l_r$ are calculated as shown in Eq. (4).

$$\int_0^{l_z} \sigma_r|_{r=l_r} 2\pi r \mathrm{d}z = F_1, \quad \int_0^{l_r} \sigma_z|_{z=l_z} 2\pi r \mathrm{d}r = F_2. \tag{4}$$

Next, the second auxiliary problem (c) shown in Fig. 3(c) is solved under the following boundary conditions:

$$\begin{aligned} &\text{(I) On } r = 0 \text{ and } 0 \leqslant z \leqslant l_z: \quad u_r = 0, \quad \tau_{rz} = 0, \\ &\text{(II) On } r = l_z \text{ and } 0 \leqslant z \leqslant l_z: \quad u_r = c_1, \quad \tau_{rz} = 0, \\ &\text{(III) On } z = 0 \text{ and } 0 \leqslant r \leqslant l_r: \quad u_z = 0, \quad \tau_{rz} = 0, \\ &\text{(IV) On } z = l_z \text{ and } 0 \leqslant r \leqslant l_r: \quad u_z = 0, \quad \tau_{rz} = 0. \end{aligned} \tag{5}$$

Then, the resultant force F_3 in the r-direction on the boundaries $r = l_r$ with $0 \leqq z \leqq l_z$, and the resultant force F_4 in z-direction on the boundaries $z = 0$, l_z with $0 \leqq r \leqq l_r$ are calculated as shown in Eq. (4).

$$\int_0^{l_z} \sigma_r|_{r=l_r} 2\pi r \mathrm{d}z = F_3, \quad \int_0^{l_r} \sigma_z|_{z=l_z} 2\pi r \mathrm{d}r = F_4. \tag{6}$$

The solution for Fig. 3(a) can be expressed by superposing the solution for Fig. 3(b) and the solution for Fig. 3(c) as shown in Eq. (7). Here the solutions of Fig. 3(a), (b), and (c) denote (σ_a, u_a), (σ_b, u_b), and (σ_c, u_c), respectively.

$$\begin{aligned} \sigma_a &= \left(\sigma_b - \frac{F_1}{F_3}\sigma_c\right) \times (\sigma_0 \times \pi l_r^2) \Big/ \left(F_2 - F_4 \frac{F_1}{F_3}\right) \\ u_a &= \left(u_b - \frac{F_1}{F_3}u_c\right) \times (\sigma_0 \times \pi l_r^2) \Big/ \left(F_2 - F_4 \frac{F_1}{F_3}\right) \end{aligned} \tag{7}$$

In this study rectangular- and cylindrical-shaped inclusions will be mainly treated because these shapes have been used as 2D and 3D models of fibers in composites. In our previous studies, for example, the magnitude of singular stress at the corner of these inclusions have been discussed [18]. The present results, however, can be applied to other shaped inclusion as shown in the next section.

3. Effect of shape of inclusion

First, plane stress condition with Poisson's ratio $\nu_M = \nu_I = 0.3$ is assumed for the matrix and inclusions, whose elastic constants are (E_M, ν_M) and (E_I, ν_I), respectively; then, square arrays of circular and elliptical inclusions are analyzed to confirm the accuracy of FEM

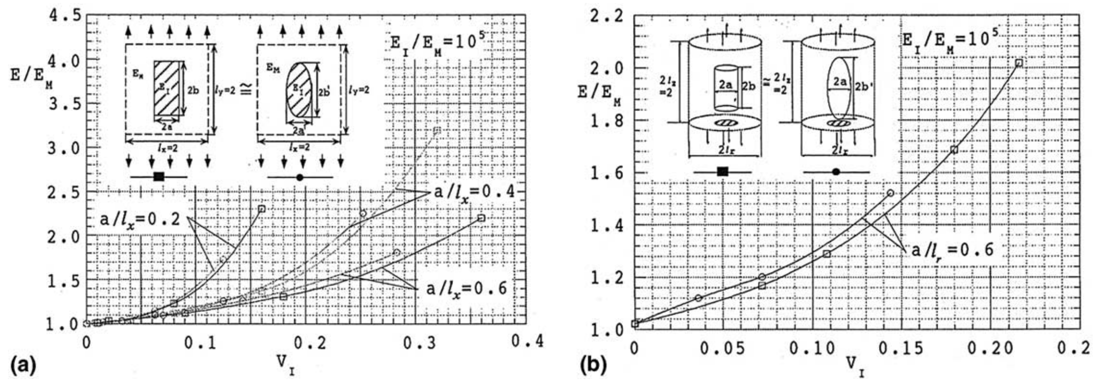

Fig. 4. (a) E/E_M vs. V_I relation for rectangular and elliptical inclusions when $l_y/l_x = 1$, $E_I/E_M = 10^5$, $\nu_M = \nu_I = 0.3$ under plane stress, (b) E/E_M vs. V_I relation for cylindrical and ellipsoidal inclusions when $l_z/l_r = 1$, $E_I/E_M = 10^5$, $\nu_M = \nu_I = 0.3$.

analysis. The present solutions for the maximum stresses coincide with Isida–Sato's [19] and Uchiyama–Yatsuda–Murakami's results [20] within 1% in most cases. In Fig. 4(a), square arrays of rectangular and elliptical inclusions are compared. In Fig. 4(b), cylindrical and ellipsoidal inclusions are compared. When the unit cell has the dimensions $2l_x \times 2l_y$, the volume fractions of inclusion $V_I = ab/(l_x l_y)$ for rectangular inclusion; and $V_I = \pi a'b'/(4l_x l_y)$ for elliptical inclusion. Here, the rectangular inclusion has dimensions a, b, and the elliptical inclusion has radii a', b'.

As shown in Fig. 4, the effective Young's modulus is not equal even though V_I = constant. The effective Young's modulus is identical under the following conditions:

(1) the projected area fractions of inclusions are equal, that is, $a/l_x = a'/l_x$;
(2) the volume fractions of inclusions are equal, that is, $ab/(l_x l_y) = \pi a'b'/(4l_x l_y)$.

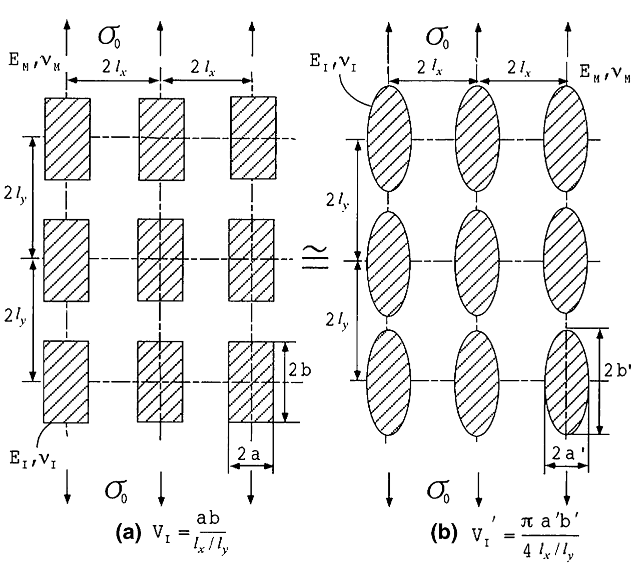

Fig. 5. Elastic modulus is almost equal when (1) $a/l_x = a'/l_x$ and (2) $ab/(l_x l_y) = \pi ab/(4l_x l_y)$.

Fig. 5 illustrates the equivalent condition of inclusions.

If the condition is satisfied, it may be concluded that the effective Young's modulus is almost equal even though the shape of inclusions differs from rectangle or ellipse. Therefore, actual irregularly shaped inclusions may be evaluated from equivalent rectangular inclusions with the application of FEM.

4. Comparison between the results of plane strain and axisymmetric unit cell models

In Fig. 6 the effective Young's moduli E are compared between the rectangular inclusions in Fig. 1(a) and cylindrical inclusions in Fig. 1(b). Here, $V_I = (a^*/l_x)(b^*/l_y)$ for plain strain model in Fig. 1(a); and $V_I = (a/l_r)^2(b/l_z)$ for axisymmetric model in Fig. 1(b). As shown in Fig. 6, the effective Young's modulus E is almost identical under the following conditions (see Fig. 7):

(1) the projected area fractions of inclusions A_I are equal, that is, $a^*/l_x = (a/l_r)2$;
(2) the volume fractions of inclusions V_I are equal, that is, $(a/l_r)^2(b/l_z) = (a^*/l_x)(b^*/l_y)$.

Using this condition we can evaluate 3D array of inclusion from the results of 2D analysis. Table 1 indicates the effect of Poisson's ratios for cylindrical and ellipsoidal inclusions when $l_y/l_x = l_z/l_r = 1$, $E_I/E_M = 10^5$. The plane strain's and axisymmetric results almost coincide with each other if the two models have the same values of A_I, V_I, Poisson's ratios ν_M, ν_I, unit cell's aspect ratio ($l_y/l_x = l_z/l_r$), and elastic ratio E_I/E_M.

5. Effect of arrangement of inclusion

In the above discussion the effective Young's modulus E is found to be controlled by two major parameters,

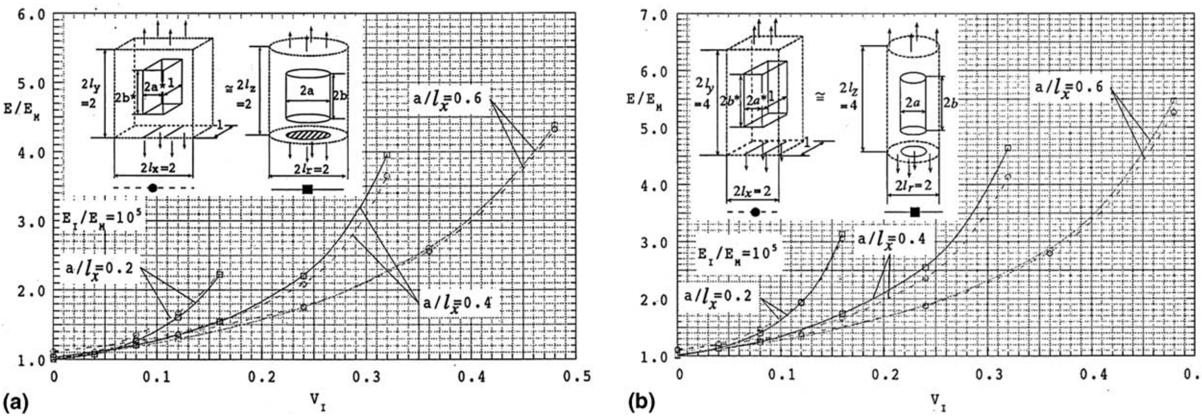

Fig. 6. (a) E/E_M vs. V_I relation for plain strain and axisymmetric inclusion models when $l_y/l_x = l_z/l_r = 1$, $E_I/E_M = 10^5$, $\nu_M = \nu_I = 0.3$ (b) E/E_M vs. V_I relation for plain strain and axisymmetric inclusion models when $l_y/l_x = l_z/l_r = 2$, $E_I/E_M = 10^5$.

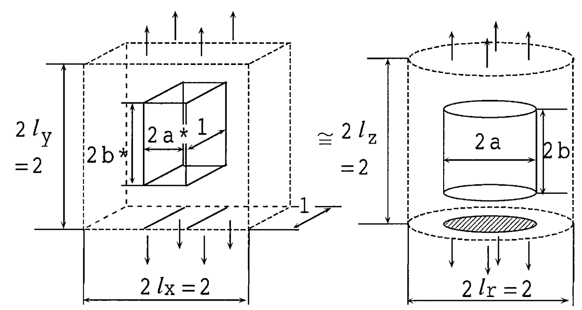

Fig. 7. Elastic modulus is almost equal when (1) the projected area fractions of inclusions are equal, that is, $a^*/l_x = (a/l_r)2$ (2) the volume fractions of inclusions are equal, that is, $(a^*/l_x)(b^*/l_y) = (a/l_r)^2(b/l_z)$.

Table 1
Effect of Poisson's ratio for cylindrical and ellipsoidal inclusions in Fig. 1(a) and (b) when $l_y/l_x = l_z/l_r = 1$, $E_I/E_M = 10^5$

Poisson's ratio ($\nu_I = \nu_M$)	0	0.3	0.4	0.45
2D Unit cell	2.829	3.057	3.547	4.087
3D Unit cell	2.951	3.134	3.592	4.141

that is, (i) the projected area fractions of inclusions A_I, and (ii) the volume fractions of inclusions V_I. This conclusion is, however, obtained from the results of two-dimensional and axisymmetric unit cell models assuming periodically arrangement of inclusions. Therefore to investigate the effect of disordered array of inclusions, the model of Fig. 1(c) is considered in this section. Here, the position of group A is fixed; then the effect of location of group B on the effective Young's modulus is considered. For the unit cell with dimensions $l_x \times l_y$, the volume fraction of inclusion is $V_I = 8ab/(l_x l_y)$ for rectangular inclusion with dimensions $2a \times 2b$. Fig. 8(a) shows dimensions of the model of periodically arranged inclusions having elastic ratio $E_I/E_M = 10^5$ and Poisson's

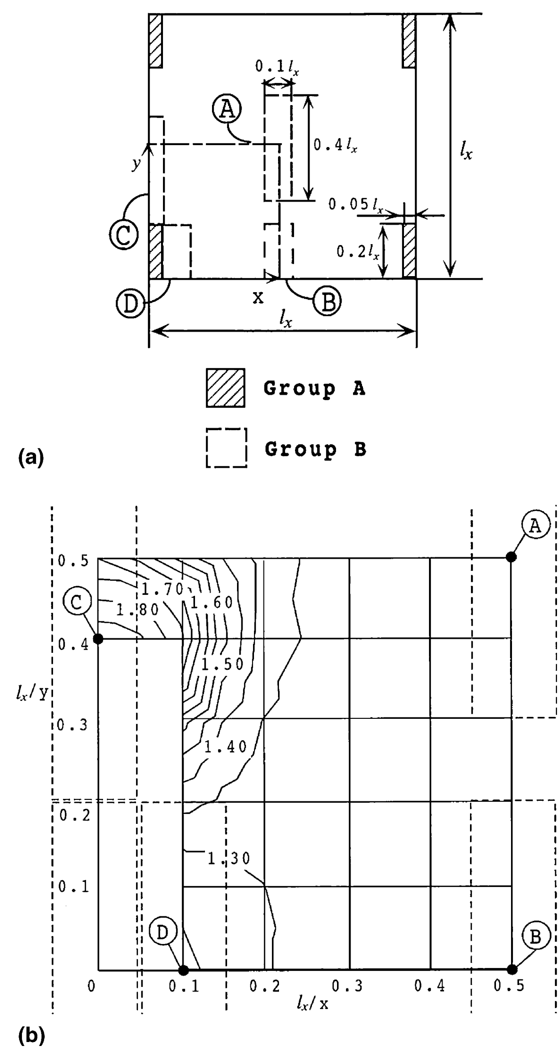

Fig. 8. (a) Dimensions of two-groups-inclusion model where both groups have the elastic ratio $E_I/E_M = 10^5$ and Poisson's ratio $\nu_M = \nu_I = 0.3$ under plane stress. (b) Effective Young's modulus E vs. the central coordinate of group B varying in the range $0 \leqq x \leqq l_x/2$, $0 \leqq y \leqq l_x/2$.

ratio $\nu_M = \nu_I = 0.3$ under plane stress. Fig. 8(b) indicates the effective Young's modulus in the y-direction E as a function of the central coordinate of group B varying in the range $0 \leqq x \leqq l_x/2$, $0 \leqq y \leqq l_x/2$. As shown in these Fig. 8, the variation of E/E_M is $0.94 \sim 1.44$; however, if we compare among the values of cases (A), (B), and (D), the variation becomes small, within about a few percent, that is, $0.94 \sim 1.02$. Therefore, it may be concluded that the effective Young's modulus is almost independent of the location of group B if the projected areas of groups A and B are not overlapped. In other words, the volume fraction of inclusion and projected area fraction of inclusions are two major parameters controlling the effective Young's modulus of model 1 (c). Therefore it may be concluded that actual composites can be evaluated efficiently in terms of two major parameters, that is, the projected area fractions and volume fractions of inclusions.

6. Conclusion

Unit cell models have been widely used to investigate mechanical properties and also ductile fracture mechanisms together with finite element analyses assuming periodically arrangement of voids, particles, inclusions, and fibers in matrix. Actual structural materials, however, usually have randomly distributed general 'inclusions'. To begin with a tractable problem, in this paper, the effect of shape and arrangement of inclusions on the effective Young's modulus E of heterogeneous materials is considered through examining three types of unit cell models as shown in Fig. 1. The conclusions can be made in the following way:

(1) The effect of shape of inclusions is considered from the results of rectangular and elliptical inclusions, together with the results of ellipsoidal and cylindrical inclusions. Then, the effective Young's modulus is found to be mainly determined by two major parameters, that is, (i) the area fraction of inclusions projected in tensile direction A_I, and (ii) the volume fraction of inclusion V_I, almost independent of shape of inclusion.

(2) The results of plane strain model in Fig. 1(a) and axisymmetric model of Fig. 1(b) are compared. Then, it is also found that the effective Young's modulus E is almost identical if (i) the projected area fractions of inclusions A_I and (ii) the volume fractions of inclusions V_I are equal.

(3) The effect of disordered array of inclusions is discussed using the model of Fig. 1(c). Here, the effect of location of group B is examined when the position of group A is fixed. Then, it may be concluded that the effective Young's modulus E is almost independent of the location of group B if the projected areas of groups A and B are not overlapped.

(4) The volume fraction of inclusion V_I and projected area fraction of inclusions A_I are found to be two major parameters controlling the effective Young's modulus of composites. Disordered irregularly-shaped inclusions may be evaluated from equivalent ordered rectangular inclusions with the application of FEM. This replacement may be effective and efficient if actual inclusions are well-approximated by elliptical, ellipsoidal, or cylindrical inclusions.

Acknowledgments

The authors wish to express their thanks to members of their group, Messrs. Takashi Wada, Ken-Ichiro Takeuchi, and Shintaro Nakaya for their much of constructional works including FEM analysis.

References

[1] Needleman A. Void growth in an elastic–plastic medium. J Appl Mech 1972;39:964–70.
[2] Tvergaad V. Influence of voids on shear band instabilities under plane strain conditions. Int J Fract 1981;17:389–407.
[3] Tvergaad V. On localization in ductile materials containing spherical voids. Int J Fract 1982;18:237–51.
[4] Christman T, Needleman A, Suresh S. An experimental and numerical study of deformation in metal–ceramic composites. Acta Metall Mater 1989;37:3029–50.
[5] Tvergaad V. Analysis of tensile properties for a whisker-reinforced metal–matrix composite. Acta Metall Mater 1990;38:185–94.
[6] Bao G, Hutchinson JW, McMeeking RM. Particle reinforcement of ductile matrices against plastics flow and creep. Acta Metall Mater 1991;39:1871–82.
[7] Zahl DB, McMeeking RM. The influence of residual stress on the yielding of metal–matrix composites. Acta Metall Mater 1991;39:1117–22.
[8] Levy A, Parazian JM. Tensile properties of short fiber-reinforced Sic/Al composites: part II. Finite element analysis. Metall Trans 1990;A21:411–20.
[9] Zhonghua Li, Schmauder S, Wanner A, Dong M. Expression to characterize the flow behavior of particle-reinforced composites based on axisymmentric unit cell modules. Scr Metall Mater 1995:1289–94.
[10] Adams DF, Doner DR. Transverse normal loading of a unidirectional composite. J Compos Mater 1967;1:152–64.
[11] Yamawaki K, Uemura M. An analysis for elastic moduli of unidirectional fiber-reinforced and multilayered composite materials. Bull Inst Space Aeronaut Sci Univ Tokyo 1971;7:315–33.
[12] Milton GW. Bounds on the transport and optical properties of a two-component composite materials. J Appl Phys 1981;52(8):5294–304.
[13] Hashin Z. Analysis of composite materials—a survey. J Appl Mech 1983;50(481):481–505.
[14] Torquato S. Modeling of physical properties of composite materials. Int J Solids Struct 2000;37(1–2):411–22.
[15] Benssousan A, Lion JL, Papanicolaou G. Asymptotic analysis for periodic structures. Amsterdam: North Holland; 1978.
[16] Sauchez-Palencia E. Lecture note in physics. Berlin: Springer; 1980.

[17] Terda K, Yuge K, Kikuchi N. Elastro-plastic analysis of composite materials using homogenization method. Trans Jpn Soc Mech Eng 1995;61(590):2199–205 (in Japanese).
[18] Noda N-A, Takase Y, Chen M-C. Generalized stress intensity factors in the interaction between two fibers in matrix. Int J Fract 2000;103:19–39.
[19] Isida M, Sato R. Analysis of finite regions containing a circular hole or inclusion with applications. Trans Jpn Soc Mech Eng 1984;50(457):1619–27 (in Japanese).
[20] Uchiyama Y, Yatsuda M, Murakami Y. Analysis of elastic moduli of a composite material containing periodically arranged elliptic inclusions. J Jpn Soc Compos Mater 1985;11(6):275–86 (in Japanese).